Exploring the Boundaries of Ambient RF Energy Harvesting With LoRaWAN

Joseph Finnegan, *Member, IEEE*, Kyriaki Niotaki, *Member, IEEE*, and Stephen Brown

***Abstract*—Environmental monitoring is an important application for wireless sensing devices. Battery power requires in-the-field replacement, and the chemicals involved are environmentally harmful, so harvested energy is a useful alternative. Previous research has shown the feasibility of powering LoRaWAN sensors using high-energy ambient or wireless transfer power sources. This article extends this work by exploring the boundaries of using low-energy radio-frequency (RF) ambient sources. Ambient RF energy harvesting is an attractive option, but it is more challenging due to the low levels of energy density typically available.Using an analytical LoRaWAN device model and RF energy data collected from around the world, a systematic investigation of the design and environmental space is performed. The main contribution of this article is to identify the boundaries of feasibility for powering LoRaWAN sensor nodes from ambient RF energy. These boundaries include design and environmental factors.**

***Index Terms*—LoRaWAN, LPWAN, radio-frequency (RF) energy harvesting (EH).**

I. Introduction

LORAWAN has recently attracted significant attention in a plethora of Internet-of-Things (IoT) applications, such as environmental monitoring. Battery usage as the main power source for LoRaWAN applications is challenging as battery power requires in-the-field replacement, and the chemicals involved are environmentally harmful, so harvested energy is a useful alternative. To overcome the battery limitations associated with LoRaWAN long scale deployment, there has been a recent interest in using energy harvesting (EH) solutions for sustaining battery-less LoRaWAN operation.

Previous research has demonstrated the feasibility of harvesting various ambient energy sources for powering LoRaWAN sensors: thermoelectric, photovoltaic, electromagnetic vibration [1]–[3], and a combination of them [4], [5]. Wireless power transmission (WPT), where dedicated radio-frequency (RF) power is transmitted, has also been considered as a potential solution in [6] and [7]. Recently, Delgado *et al.* [8] investigated the operation of a battery less, EH LoRaWAN device in the context of relatively high harvested power levels. All of these approaches have considered relatively high levels of energy, and address the issue primarily by identifying a single solution that works.

Manuscript received August 18, 2020; revised September 7, 2020; accepted October 8, 2020. Date of publication October 13, 2020; date of current version March 24, 2021. This work was supported in part by the Science Foundation Ireland and in part by the European Regional Development Fund under Grant 13/RC/2077. *(Corresponding author: Kyriaki Niotaki.)*

Joseph Finnegan and Stephen Brown are with the Department of Computer Science, Maynooth University, W23 F2H6 Maynooth, Ireland.

Kyriaki Niotaki is with the Department of Electronic Engineering, Maynooth University, W23 F2H6 Maynooth, Ireland (e-mail: nkiriaki@gmail.com).

Digital Object Identifier 10.1109/JIOT.2020.3030349

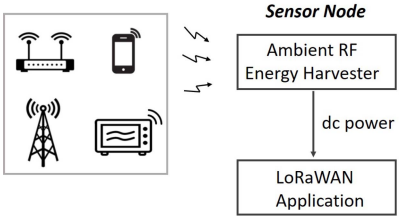

Fig. 1. Real-life ambient RF EH scenario where many existing RF sources are present.

In contrast to the previous work, this article investigates the significantly more difficult issue of exploiting low level, *ambient* RF power to sustain autonomous operation of LoRaWAN devices. The approach taken is to identify the boundaries of feasibility by exploring the impact of various device and environmental parameters on the feasibility of operation. Ambient RF EH, as opposed to WPT, refers to the usage of available RF energy from existing sources, such as TV broadcasts, radio base stations, and cellular phones, as shown in Fig. 1. The ambient RF energy is collected from the energy harvester which converts it to useful dc energy for LoRaWAN applications.

The main advantage of RF EH over WPT is that the power does not have to be purposely provided by the operator of the harvester and thus constitutes a "free" energy source. However, RF EH is considered one of the most challenging energy sources as the available harvestable power varies over frequency, time and location, with the distance from the energy source, and as a result of various environmental conditions. Additionally, the power density available through RF EH is low compared with other renewable energy sources [9]. As highlighted by the recent survey [10], there is currently no published work which analyses the potential of powering LoRaWAN applications through ambient RF EH. The novelty in the work presented here is the systematic exploration of the design and environmental space to identify the boundaries of viability of RF EH powered LoRaWAN, based on real-life energy data.

Initially, an analytical model of the energy consumption of a representative device is developed. Based on this model, the analysis of a typical ambient RF EH environment and RF

energy data from around the world, the feasibility of using ambient RF EH to sustain the operation of LoRaWAN devices is demonstrated. A number of limitations related to design and environmental factors are identified.

This work is structured as follows. Section II describes the analytical model of a typical LoRaWAN device. Section III introduces RF EH principles and presents real-life RF EH data. In Section IV, the feasibility of RF EH with LoRaWAN is investigated and the obtained results are presented. Section V concludes this article and provides some discussion on the results.

II. LoRaWAN Analytical Model

The modeling of the power consumption of a LoRaWAN device presented here is based on a system-level approach [11], including the full LoRaWAN protocol. The power consumed by an LPWAN device can be separated into four constituent parts

$$P_{\text{system}} = P_{\text{sens}} + P_{\text{net}} + P_{\text{prc}} + P_{\text{sys}}. \tag{1}$$

A. Sensing (P_{sens})

The energy consumption required for sensing depends on the sampling rate, duration, and current consumption of the sensor. The use case considered requires a single reading immediately prior to the transmission of an uplink frame, leading to the expression

$$P_{\text{sens}} = \frac{E_{\text{sample}}}{t} \tag{2}$$

where $t = t_{\text{periodicity}}$ is the periodicity of uplink transmissions and E_{sample} is the energy consumption to take one reading from a sensor.

B. Networking (P_{net})

The energy consumption of the networking side of a LoRaWAN module is dependent on six primary factors: the packet size, the transmission rate of uplink and downlink frames, the transmission power of the transceiver, the device class, and the data rate used by the device. Use of a slower data rate results in a larger range but also a longer transmission time and less energy efficient transmission. The LoRaWAN adaptive data rate (ADR) scheme adjusts the data rate based on recent traffic. In the model, it is assumed the device has settled to a particular data rate, and thus this is taken as an input parameter. Use of LoRaWAN Class A is modeled as this class defines an ALOHA-based MAC layer that is the most suited to applications with energy constraints and minimal downlink requirements.

1) LoRaWAN Class A: The format of a Class A transmission is shown in Fig. 2. Following every Class A transmission the device opens two receive windows. With the default LoRaWAN configuration, in the first receive window (*RX*1), the device waits for a downlink frame on the same channel and data rate as the preceding uplink frame. In the second receive window (*RX*2), the device waits for a downlink frame using a predefined channel and data rate (by default DR0, the lowest data rate). A receive window is opened for long enough to detect a preamble. If a preamble is detected, the device continues to receive the entire frame. It can therefore be concluded that in modeling the energy consumption of a Class A frame there are three different situations which must be considered: 1) an unresponded frame; 2) a frame responded to in *RX*1; and 3) a frame responded to in *RX*2.

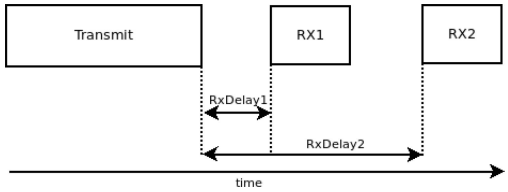

Fig. 2. LoRaWAN Class A transmission.

2) LoRaWAN Transmission Time: The Time-on-Air of a LoRaWAN packet can be calculated by summing the transmission times of the preamble and the payload [12]

$$t_{\text{packet}} = t_{\text{pre}} + t_{\text{payload}}. \tag{3}$$

LoRaWAN packets by default contain a preamble of 8 symbols (N_{pre}), the transmission time of which is directly dependent on the bandwidth (*BW*) and spreading factor (*SF*), which are both specified by the data rate

$$t_{\text{pre}} = \left(N_{\text{pre}} + 4.25\right) * \left(2^{\text{SF}}\right)/BW. \tag{4}$$

The transmission time of the payload is dependent on the data rate and number of symbols required

$$t_{\text{payload}} = p_{\text{sym}} * \left(2^{\text{SF}}\right)/BW. \tag{5}$$

The number of symbols is based on the length of the payload in bytes (*PL*), the spreading factor, and the code rate (*CR*)

$$p_{\text{sym}} = 8 + \max\left(\text{ceil}\left(\frac{8PL - 4\text{SF} + 44 - 20H}{4 * (\text{SF} - 2DE)}\right) * (\text{CR} + 4), 0\right) \tag{6}$$

where *H* indicates the existence of a physical header (0 when the header is enabled), and *DE* the use of low data rate optimisation, which is present only in transmissions using DR0 and DR1, the lowest data rates.

3) Unresponded Frame: From Fig. 2, it can be seen that the behavior by state for an unresponded LoRaWAN Class A transmission consists of an uplink transmission (*tx*), and the opening of two receive windows just long enough to read a preamble (*rx1Pre* and *rx2Pre*), with the device remaining in standby mode for the in-between wait states (*ww1* and *ww2*). Thus, the total energy consumption is directly dependent on the current consumption and length of time in each state

$$\begin{aligned} E_{\text{UnresA}} = (&t_{tx} * I_{tx} + t_{ww1} * I_{\text{std}} + t_{rx1Pre} * I_{rx} \\ &+ t_{ww2} * I_{\text{std}} + t_{rx2Pre} * I_{rx}) * Vcc. \end{aligned} \tag{7}$$

Since downlink traffic in LoRaWAN is limited, this is by far the most common behavior for a Class A transmission. Note that the length of time in the *ww2* state is dependent on the data rate used in the uplink transmission.

4) Responded Frame in RX1: When a transmission is responded to in *RX*1, *ww1* and *RX*2 are skipped, and so the total energy consumption is

$$E_{ResA\_RX1} = (t_{tx} * I_{tx} + t_{ww1} * I_{\text{std}} + t_{rx1Recv} * I_{rx}) * Vcc. \quad (8)$$

5) Responded Frame in RX2: And finally, when a transmission is responded to in *RX*2, the total energy consumption is

$$E_{ResA\_RX2} = (t_{tx} * I_{tx} + t_{ww1} * I_{\text{std}} + t_{rx1Pre} * I_{rx} + t_{ww2} * I_{\text{std}} + t_{rx2Recv} * I_{rx}) * Vcc. \quad (9)$$

6) Proportional Usage of RX1 and RX2: In current Network Server implementations *RX*1 is used as a priority for downlink responses, duty cycle regulations permitting. For smaller networks with minimal downlink responses, *RX*1 will be predominantly used. In the model, an *RX*2 usage rate of 5% is applied, corresponding to a relatively small LoRaWAN network. This leads to an average energy consumption in a responded LoRaWAN frame of

$$E_{\text{ResA}} = \frac{E_{\text{ResA\_RX1}} * 19 + E_{ResA\_RX2}}{20}. \quad (10)$$

7) Expected Downlink Traffic: In the model, the sending of minimal downlink traffic is assumed, i.e., downlink frames are sent as a result of the ADR scheme only. Using the standard LoRaWAN ADR configuration, this results in a downlink transmission every 32 frames in the most pessimistic case. Thus, the average energy consumption of a LoRaWAN transmission for a particular device can be calculated as

$$E_{\text{packet}} = \frac{31 * E_{\text{UnresA}} + E_{\text{ResA}}}{32} \quad (11)$$

and as LoRaWAN Class A is an ALOHA-based protocol, the power consumption for the networking side of the system can be defined purely based on the energy consumption for an individual packet and the transmission periodicity $t = t_{\text{periodicity}}$

$$P_{\text{net}}(t, \text{DR}) = \frac{E_{\text{packet}}(\text{DR})}{t}. \quad (12)$$

C. Data Processing (P_{prc}) and Other System Tasks (P_{sys})

Similarly to the LoRa use case described in [11], as a simple reporting application is modeled, the processing load is very low, and so this factor can be omitted. The remaining energy consumption is dependent on the remaining time per transmission period when not transmitting or sensing, where the device is in the lowest power state

$$E_{\text{sleep}}(t, \text{DR}) = I_{\text{sleep}} * \left(t - t_{\text{packet}}(\text{DR}) - t_{\text{sense}}\right) * Vcc. \quad (13)$$

D. Power Consumption Model

Finally, the preceding formulas can be recombined to redefine (1)

$$P_{\text{system}}(t) = P_{\text{sens}}(t) + P_{\text{net}}(t, \text{DR}) + P_{\text{prc}}(t) + P_{\text{sys}}(t) = \frac{E_{\text{sample}} + E_{\text{packet}}(\text{DR}) + E_{\text{sleep}}(t, \text{DR})}{t} \quad (14)$$

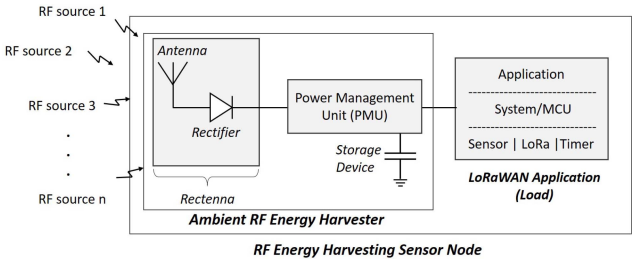

Fig. 3. General structure of a typical ambient RF EH LoRaWAN system.

which defines the average amount of energy consumed by the entire system in a time period t, where there is only one transmission in the period. Additionally, the total amount of energy consumed by the system in that time period is

$$E_{\text{system}}(t) = E_{\text{sample}} + E_{\text{packet}}(\text{DR}) + E_{\text{sleep}}(t, \text{DR}). \quad (15)$$

III. Radiofrequency Energy Harvesting

Next, the general structure of a typical ambient RF EH environment is analyzed. The approach taken is to first quantify the available dc power based on RF measurement campaigns worldwide. Then, an analytical model of a real-life EH environment where an RF energy harvester scavenges power over time from various existing RF sources is analyzed. The impact of each EH component (rectenna, power management unit (PMU) and storage device) on the system performance is discussed. Finally, an aggregated energy model is presented, taking into account the total amount of energy consumed by the system, as discussed in the previous section.

A. Ambient RF Power Level

The term RF EH refers to the usage of available RF energy from existing RF sources (as shown in Fig. 1). The available RF energy is collected from an energy harvester that converts it to dc energy to supply the LoRaWAN application. Fig. 3 shows the structure of a typical RF EH LoRaWAN node. Each of these components are discussed later in this section.

To quantify the power level availability, a series of measurement campaigns have been conducted. The results are either expressed in terms of ambient RF channel power density levels (usually measured in dBm/cm^2) or as the input power level at the antenna (measured in dBm or W), as shown in Fig. 3. The measured power level at the antenna of the energy harvester device is used in this analysis.

The ambient RF power level in China was measured within the frequency range of 0.7–3 GHz outside a shopping mall and in residential areas in [13]. Lim *et al.* [14] evaluated the RF power density at GSM bands in Singapore with a peak power level of −31 dBm. Guenda *et al.* [15] measured a peak power level of −32 dBm and −22 dBm half a meter from a mobile phone and a microwave oven, respectively. A set of indoor and outdoor measurements at Universidad Politecnica de Madrid (UPM) have also been carried out recently in Madrid [16]. Fig. 4 summarizes the peak measured indoor and outdoor power level at various frequencies in different locations around

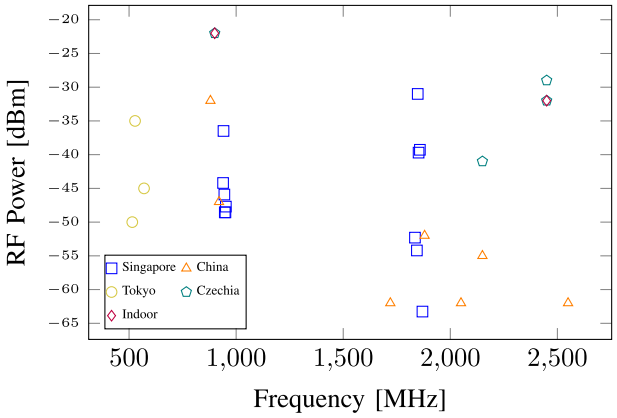

Fig. 4. Measured indoor and outdoor environmental power level at single frequencies around the world [13]–[15], [17], [18].

the world. Closely spaced data points for the same location represent slightly different frequencies.

Although the measurements shown in Fig. 4 give an indication of the power level across a frequency band, to calculate the total instantaneous power across a wireless channel (from f_l to f_h), the following formula can be used:

$$P_{\text{RFchan}} = \int_{f_l}^{f_h} P_{RF(f)} df \tag{16}$$

where $P_{RF(f)}$ is the spectral power from f_l to f_h. Indeed, wider signals have the potential to accumulate more power if compared with narrower signals [14]. As an example, in [18] and [19] the authors carried out measurement campaigns in downtown Japan and USA, respectively, from 50 to 900 MHz and measured a peak carrier power level of −35 dBm at 6.3 km away from a TV broadcast source. However, across the band, the total measured power level was −8.99 dBm.

As the available ambient RF power comes from various RF sources, the total instantaneous power from the multiple sources is an aggregate of the harvested power per each frequency channel

$$P_{\text{RFtot}} = \sum_{i=c_1}^{c_n} P_{\text{RFchan}(i)} \tag{17}$$

where $P_{\text{RFchan}(i)}$ is the harvested power from each frequency channel $(c_1, \ldots, c_n)$. Due to its nature, ambient power can fluctuate over time. According to some recent measurements in Houston, the ambient RF power is relatively stable in the time-domain, however the available RF power is less stable during the daytime due to the activities of people [20], [21]. In each case, the available RF energy level in a time interval (from t_1 to t_2) can be calculated as [22]

$$E_{\text{RFtot}}(t) = \int_{t_1}^{t_2} P_{\text{RFtot}(t)} dt \tag{18}$$

where $P_{\text{RFtot}(t)}$ is the RF power distribution versus time and indicates the energy harvester input power level (Fig. 3). Table I shows the total measured RF power P_{RFtot} in various locations. For an easy illustration and comparison, from now on, all power levels will be expressed in W rather than dBm.

TABLE I
TOTAL AMBIENT RF POWER AND HARVESTED DC POWER

Measurement Scenario	Available RF Power	Harvested dc Power
6.3km from TV Tower in Tokyo (512-566 MHz) [18]	126 μW	16 μW
Base stations & Wi-Fi Hotspots (London underground) [23] [24]	-	1-50 μW
Inside UPM (0.1-6 GHz) [16]	480 μW	-
Outside UPM (0.1-6 GHz) [16]	1535 μW	-
Inside UPM(770-820&920-970MHz) [16]	380 μW	-
Outside UPM(770-820&920-970MHz) [16]	1300 μW	>80 μW *

* Exact dc power not shown in this paper.

B. Rectenna

To scavenge RF power, a rectifying antenna (or rectenna) is needed to collect the RF power and convert it to useful dc power [25]. Rectennas usually consist of an antenna and a rectifier at its simplest form (as in Fig. 3). The harvested dc power depends on the efficiency of the rectenna. The RF-to-dc conversion efficiency of the rectenna depends on its operating bandwidth; narrower rectennas tend to be more efficient [26]. Also, the RF-to-dc conversion efficiency depends on the output dc voltage and the RF input power level; for example, it can be in the order of 10% and 40% for 10 μW and 1 mW, respectively, [27], [28]. To minimize the sensitivity of the rectifier on these parameters, novel circuits have been proposed in [28]. Table I shows the aggregated dc power as measured in various locations worldwide. Note that the dc power is a few orders less than the RF power due to the low RF-to-dc efficiency of the rectenna. Based on these measurements, this article uses a range of 10 to 80 μW to represent a reasonable range of achievable dc power levels. This harvested power is used as an input parameter in the energy model. In this work, as a simplification, and due to the lack of high-granularity data on the energy variation reported in the measurement campaigns, an average figure is used. This is a reasonable approximation as the device is in the sleep state for long periods of time, and the integral of the energy harvested over this long period will be the same whether the actual energy level varies or not during this time. The energy harvested during a time interval (δt) can be calculated using (19)

$$E_{\text{harv}}(t) = P_{\text{harv}} * \delta t. \tag{19}$$

C. Power Management Unit

The microwatts (μW) of harvested dc power can be managed from PMUs in conjunction with an energy storage element. The PMU circuitry can include boost-up/boost-down converters and/or regulators and can be either an off-the-shelf solution or custom made board [29]. Loubet *et al.* [6] used the off-the-shelf PMU BQ25504 for LoRaWAN, while in [30] the PMU LTC3108 is used in an EH system collecting energy from Wi-Fi networks.

A PMU can increase the effective use of harvested power by using maximum power point tracking (MPPT) techniques [31], and by regulating the output voltage (which also decreases the current consumed by the load, e.g., the CPU and transceiver). However, a PMU also consumes a small current to operate -

this can become a significant factor when the load is in sleep mode. Also, any boost-up/boost-down and regulation operation are subject to losses, typically characterized by an efficiency figure for the PMU.

The following equation is used in this work to study the impact of a PMU on the harvested power requirement. It reflects the relative energy used when compared to a system with no PMU

$$E_{\text{pmu}} = E_{\text{nopmu}} * \left(1.0 + f_{\text{pmu}}\right) \tag{20}$$

where

$$E_{\text{nopmu}} = E_{\text{system}} + E_{\text{leak}}. \tag{21}$$

The factor f_{pmu} reflects the relative net loss or gain provided by the PMU operation. For no PMU, f_{pmu} has the value 0, for a net loss it is positive, and for a net gain is negative.

D. Storage Device

Capacitors, supercapacitors, batteries or a combination of the three can be used as the storage mechanism. Each storage option comes with advantages and disadvantages [32]. In this work, a single supercapacitor is adopted as the storage device due to its long life-time and in accordance with the required capacitance level. The maximum energy storage capability (E) depends on the capacitance C, as shown in the following equation:

$$E = \frac{C}{2} * (V_{\text{rated}})^2 \tag{22}$$

where V_{rated} is the rated voltage of the capacitor, as per the manufacturer datasheet. However, in reality, a capacitor will operate across a range of useful voltages (from V_{min} to V_{max}) and the stored energy level will be

$$E = \frac{C}{2} * \left(V_{\text{max}}^2 - V_{\text{min}}^2\right). \tag{23}$$

While large capacitors can store a large amount of energy, a long time is taken to charge/discharge and part of the stored energy is lost due to the leakage current $I_{\text{leak}}(t)$. The supercapacitor leakage power depends on the operating voltage and temperature, however in this work, for simplicity, the supercapacitor leakage power $E_{\text{leak}}(t)$ is considered to be constant (as per the datasheet), as also shown in [33] and [34].

E. Combined Energy Model

The energy level without a PMU in the storage device at a specific time $t + \delta t$ can be modeled as shown in the following equation:

$$E(t + \delta t) = E(t) + E_{\text{harv}}(\delta t) - E_{\text{system}}(\delta t) - E_{\text{leak}}(\delta t) \tag{24}$$

where $E_{\text{harv}}(\delta t)$ is the harvested dc energy and comes from Table I, $E_{\text{system}}(\delta t)$ is the energy consumed by the load (LoRa, MCU, sensor, and timer) and defined in (15), and $E_{\text{leak}}(\delta t)$ is the energy loss due to the supercapacitor leakage current $I_{\text{leak}}(t)$ [35]. The voltage on the storage device (without a PMU) can be calculated at time $t + \delta t$ using the standard equation shown in the following equation:

$$V(t + \delta t) = \sqrt{2 * E(t + \delta t)/C}. \tag{25}$$

TABLE II
REFERENCE PARAMETERS

Name	Value	Comment
Min operating voltage	2.7 V	SX1276 lower limit
Max operating voltage	3.7 V	ATmega32U4 upper limit
Base sleep current	510 nA	ATmega32U4, SX1276, PCF2123 Specifications
Storage capacitance	320 mF	GW109F
Base leakage current	1 μA	GW109F
Transmitting	35.5 mA	SX1276 at 14 dBm
Receiving	17 mA	SX1276
Standby	6.6 mA	SX1276
CPU only (active at 4 MHz)	5 mA	ATmega32U4
Sensor Sample	13.8 mA	SHT3x-DIS
Sensor Sample Time	0.0132 s	SHT3x-DIS

The following equation shows the stored energy level at a specific time $t + \delta t$ when a PMU is included

$$E(t + \delta t) = E(t) + E_{\text{harv}}(\delta t) - E_{\text{pmu}}(\delta t). \tag{26}$$

The output voltage of the PMU is fixed in this case.

IV. RESULTS

The results shown in this section are calculated using the energy model presented in the previous section. The energy is calculated over a sleep-sense-and-transmit cycle of length $t = t_{\text{periodicity}}$. This assumes a single sense operation, a single packet (5-B payload) sent, and a recharging/sleep time per cycle (send-and-transmit cycle). The minimum and maximum voltages are calculated using (25).

A base-level/reference device is used to evaluate the feasibility of a LoRaWAN node powered entirely from harvested RF energy. This is loosely based on the BSFrance LoRa32u4II board (SX1276 LoRa transceiver, ATmega32U4 CPU) with an external PCF2123 wakeup timer, GW109F supercapacitor, SHT3x-DIS temperature and humidity sensor [36].

The use of an external wake-up timer enables a super low power sleep mode for the device when not in a transmission cycle. The values used for the baseline calculations are shown in Table II. Note that the leakage and sleep current are varied in subsequent results to show the feasibility of such a node for variations in these values. The sensor was isolated from the voltage supply using an FET isolation switch to minimise the sleep current. An empirical characterization of the sensor was performed to calculate the sensor sample current and time. Baseline calculations are presented with and without a PMU.

A. Base-Level Results

Fig. 5 shows the stored energy versus time for each of the data rates over one sense-and-transmit cycle using the baseline parameters. The energy level starts at a value that matches the lowest operating voltage (2.7 V), and gradually increases until enough energy is stored to perform a single sense and transmit operation. The energy level required is greatest for DR0, the slowest data rate, and smallest for DR5, the fastest data rate. The energy then drops back to the initial energy value over the short period of time required for the sense-and-transmit operation. Note that in practice, a node would monitor

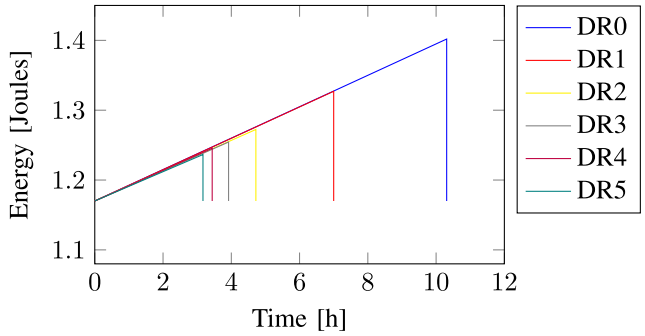

Fig. 5. Stored energy versus time over 1 cycle for each data rate.

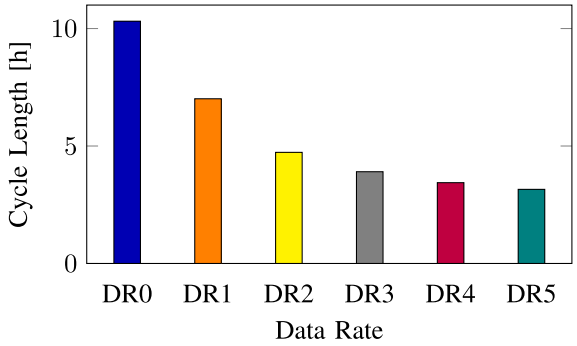

Fig. 6. Cycle lengths (sense-and-transmit) at 10-μW harvested power.

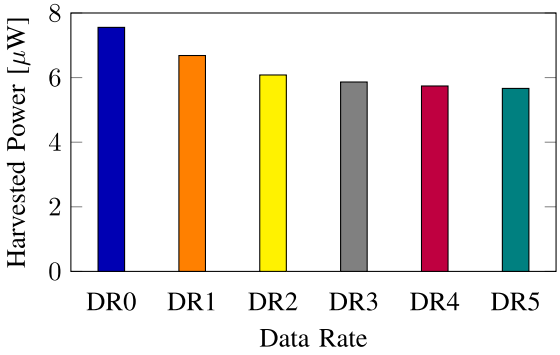

Fig. 7. Required harvested power for 1 sense-and-transmit cycle per day.

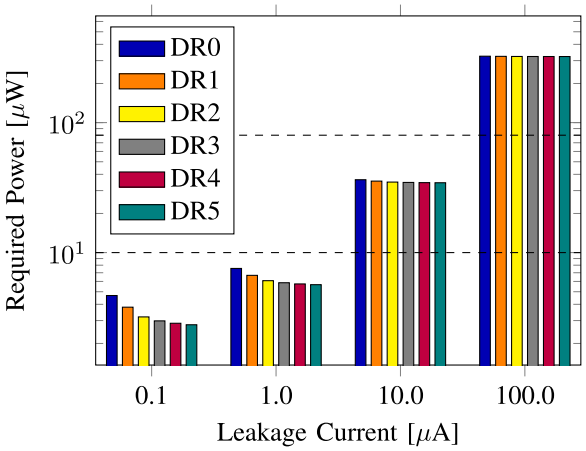

Fig. 8. Log plot showing the effect of leakage current on the required power.

the stored energy level, and only start a sense-and-transmit operation once it was sufficient for the current data rate.

Fig. 6 shows the base-level sense-and-transmit cycle period for the different data rates, using a value for the harvested energy of 10 μW, which is at the low end of what the reviewed papers have measured. This result shows that a sensor in such an environment can operate using harvested wireless power with a period between 4 h and 10 h. Note that the shortest and longest cycles different by a factor of 2.5—the data rate has a significant impact on the cycle time.

B. Sensitivity Results

A baseline is shown in Fig. 7, which shows the required level of power that must be harvested in order to achieve one sense-and-transmit cycle per day at the different LoRaWAN data rates. Note that the increased losses during the sleep phase of the cycle make the power levels less sensitive to the data rate. The highest data rate requires just under 6 μW, and the lowest data rate requires just under 8 μW.

The capacitor leakage current is a significant limiting factor. The sensitivity of the results to this leakage current is shown in Fig. 8. The dotted lines highlight the 10 μW and 80 μW power levels: from the RF EH results in the literature, results below 10 μW are regarded as having a high degree of feasibility, and results above 80 μW as having a low degree. This figure shows two results. By comparing the required energy level across the data rates for each leakage current, it can be seen that the transmit power has relatively little impact for leakage currents over 1 μA, and more impact for low leakage currents. However, at high leakage currents the leakage current dominates the power budget, and based on the reported figures for harvested wireless power, it is unlikely to be feasible to operate from harvested energy alone with a leakage current significantly over 10 μA.

The sleep current (for the CPU and LoRa transmitter) is another significant limiting factor. The baseline results use a relatively low current, based on placing the CPU into its deepest sleep mode with a programmable external clock as described. The sensitivity of the results to the sleep current is shown in Fig. 9. The dotted lines again highlight the 10 and 80-μW power levels. These results show that with the measured levels of harvested power (from 10 to 80 μW), a sensor node can support sleep mode currents slightly greater than 5 μA as long as the leakage current is low.

C. Sensitivity Results (With PMU)

The results shown previously do not include a PMU. Energy losses and inefficiencies in the PMU may be expected to reduce the effectiveness of these devices at the very low power levels typical of wireless harvesting. Fig. 10 is calculated using (26) to account for the impact of the PMU, which may produce an overall reduction (Net Gain) or increase (Net Loss) in the amount of power (in μW) required to be harvested by the device to operate at one cycle per day, compared to a device with no PMU, as discussed in Section III-C. The calculations for a net 50% gain show that a device can operate

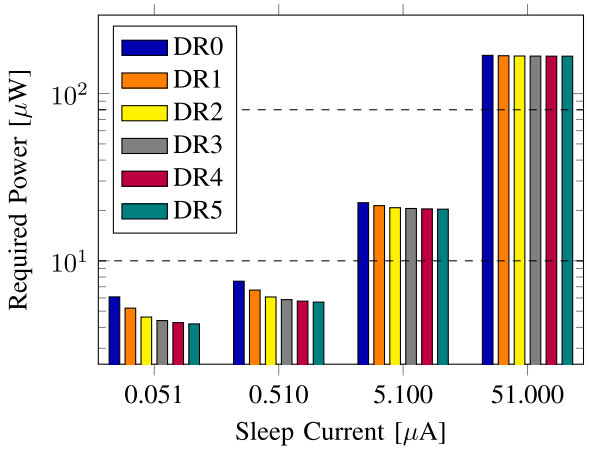

Fig. 9. Log plot showing the effect of sleep current on the required power.

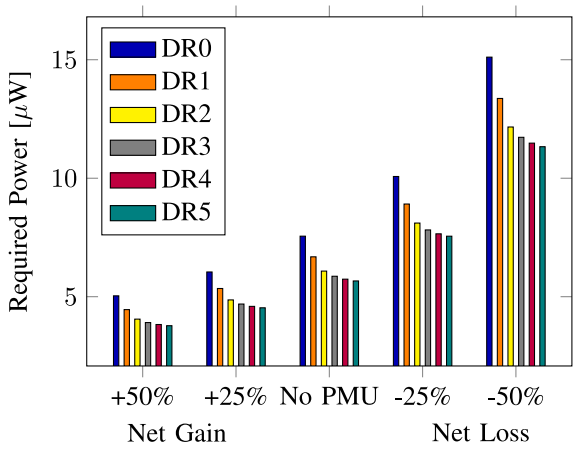

Fig. 10. Effect of PMU efficiency on the required power.

at 1 cycle per day down to 5 μW of harvested power. The calculations for a net 50% loss show that the required power to be harvested increases up to 15 μW.

V. Conclusion

The contribution of this article is to identify the boundaries of feasibility for using ambient RF EH for LoRaWAN sensor nodes. Four key design factors are identified: 1) the required sense-and-transmit cycle length for the application; 2) the leakage current; 3) the sleep current; and 4) the effect of a PMU. Two key environmental factors are also identified: 1) the level of available ambient wireless energy in the waveband used by the energy harvester and 2) the distance from the base station (and background noise level), which determines the data rate (DR0-DR5) used, and thus the energy required to transmit a frame.

Based on published, real-world measurements of levels of harvestable energy at various locations worldwide, the results show that many urban locations have the potential to support daily, short-distance measurement reporting. Longer distance communications, or more frequent reporting intervals, are shown to not always be sustainable through ambient RF EH only—i.e., where they exceed the boundaries of feasibility. Recently published results have shown that LoRaWAN sensor nodes are feasible using the higher levels of harvestable energy associated with solar and thermal energy for example, but this work identifies the conditions under which they can be also feasible at the lower energy levels associated with ambient RF harvesting. As hardware becomes more efficient, the design boundaries will change, making such scenarios ever more feasible—for example, using the newer generation of LoRa transceivers (SX126* class). The importance of conducting site environmental surveys in order to determine whether the harvestable RF energy levels are sufficient for successful deployment is also emphasized.

The main contribution of this work is to provide a systematic basis for the development of LoRaWAN-based sensor node platforms for environmental monitoring-style applications using ambient RF EH.

References

[1] M. Mabon, M. Gautier, B. Vrigneau, M. Le Gentil, and O. Berder, "The smaller the better: Designing solar energy harvesting sensor nodes for long-range monitoring," *Hindawi Wireless Commun. Mobile Comput.*, vol. 2019, Jul. 2019, Art. no. 2878545.

[2] D. Purkovic, M. Hönsch, and T. R. M. K. Meyer, "An energy efficient communication protocol for low power, energy harvesting sensor modules," *IEEE Sensors J.*, vol. 19, no. 2, pp. 701–714, Jan. 2019.

[3] F. Orfei, C. Benedetta Mezzetti, and F. Cottone, "Vibrations powered LoRa sensor: An electromechanical energy harvester working on a real bridge," in *Proc. IEEE SENSORS*, Orlando, FL, USA, Oct. 2016, pp. 1–3.

[4] M. Magno, F. A. Aoudia, M. Gautier, O. Berder, and L. Benini, "WULoRa: An energy efficient IoT end-node for energy harvesting and heterogeneous communication," in *Proc. Design Autom. Test Eur. Conf. Exhibit. (DATE)*, Lausanne, Switzerland, Mar. 2017, pp. 1528–1533.

[5] W. Lee, M. J. W. Schubert, B. Ooi, and S. J. Ho, "Multi-source energy harvesting and storage for floating wireless sensor network nodes with long range communication capability," *IEEE Trans. Ind. Appl.*, vol. 54, no. 3, pp. 2606–2615, May/Jun. 2018.

[6] G. Loubet, A. Takacs, E. Gardner, A. De Luca, F. Udrea, and D. Dragomirescu, "LoRaWAN battery-free wireless sensors network designed for structural health monitoring in the construction domain," *Sensors*, vol. 19, p. 1510, Mar. 2019.

[7] S. Tjukovs, J. Eidaks, and D. Pikulins, "Experimental verification of wireless power transfer ability to sustain the operation of LoRaWAN based wireless sensor node," in *Proc. Adv. Wireless Opt. Commun. (RTUWO)*, Riga, Latvia, Nov. 2018, pp. 83–88.

[8] C. Delgado, J. M. Sanz, and J. Famaey, "On the feasibility of battery-less LoRaWAN communications using energy harvesting," in *Proc. IEEE Global Commun. Conf. (GLOBECOM)*, Waikoloa, HI, USA, Dec. 2019, pp. 1–6.

[9] S. Kim, M. Lee, and C. Shin, "IoT-based strawberry disease prediction system for smart farming," *Sensors*, vol. 18, no. 11, p. 4051, 2018.

[10] G. Peruzzi and A. Pozzebon, "A review of energy harvesting techniques for low power wide area networks (LPWANs)," *Energies*, vol. 13, no. 13, p. 3433, 2020.

[11] B. Martinez, M. Montón, I. Vilajosana, and J. D. Prades, "The power of models: Modeling power consumption for IoT devices," *IEEE Sensors J.*, vol. 15, no. 10, pp. 5777–5789, Oct. 2015.

[12] *SX1272/3/6/7/8: LoRa Modem Designer's Guide*, Semtech, Camarillo, CA, USA, Jul. 2013.

[13] A. S. Andrenko, X. Lin, and M. Zeng, "Outdoor RF spectral survey: A roadmap for ambient RF energy harvesting," in *Proc. IEEE Region 10 Conf. (TENCON)*, Macao, China, Nov. 2015, pp. 1–4.

[14] T. B. Lim, N. M. Lee, and B. K. Poh, "Feasibility study on ambient RF energy harvesting for wireless sensor network," in *Proc. IEEE MTT-S Int. Microw. Workshop Series RF Wireless Technol. Biomed. Healthcare Appl. (IMWS-BIO)*, Singapore, Dec. 2013, pp. 1–3.

[15] L. Guenda, E. Santana, A. Collado, K. Niotaki, N. Carvalho, and A. Georgiadis, "Electromagnetic energy harvesting—Global information database," *Trans. Emerg. Telecommun. Technol.*, vol. 25, pp. 56–63, Jan. 2014.

[16] A. Alex-Amor *et al.*, "RF energy harvesting system based on an archimedean spiral antenna for low-power sensor applications," *Sensors*, vol. 19, p. 1318, Mar. 2019.
[17] M. Mrnka, P. Vasina, M. Kufa, V. Hebelka, and Z. Raida, "The RF energy harvesting antennas operating in commercially deployed frequency bands: A comparative study," *Int. J. Antennas Propag.*, vol. 2016, pp. 1–11, Apr. 2016.
[18] R. J. Vyas, B. B. Cook, Y. Kawahara, and M. M. Tentzeris, "E-WEHP: A batteryless embedded sensor-platform wirelessly powered from ambient digital-TV signals," *IEEE Trans. Microw. Theory Techn.*, vol. 61, no. 6, pp. 2491–2505, Jun. 2013.
[19] R. Shigeta *et al.*, "Ambient RF energy harvesting sensor device with capacitor-leakage-aware duty cycle control," *IEEE Sensors J.*, vol. 13, no. 8, pp. 2973–2983, Aug. 2013.
[20] Y. Luo, L. Pu, G. Wang, and Y. Zhao, "RF energy harvesting wireless communications: RF environment, device hardware and practical issues," *Sensors*, vol. 19, p. 3010, Jul. 2019.
[21] Y. Chapre, P. Mohapatra, S. Jha, and A. Seneviratne, "Received signal strength indicator and its analysis in a typical WLAN system (short paper)," in *Proc. 38th Annu. IEEE Conf. Local Comput. Netw.*, Sydney, NSW, Australia, Oct. 2013, pp. 304–307.
[22] M. Prauzek, J. Konecny, M. Borová, K. Janosová, J. Hlavica, and P. Musilek, "Energy harvesting sources, storage devices and system topologies for environmental wireless sensor networks: A review," *Sensors*, vol. 18, p. 2446, Jul. 2018.
[23] M. A. Andersson, A. Özçelikkale, M. Johansson, U. Engström, A. Vorobiev, and J. Stake, "Feasibility of ambient RF energy harvesting for self-sustainable M2M communications using transparent and flexible graphene antennas," *IEEE Access*, vol. 4, pp. 5850–5857, 2016.
[24] M. Piñuela, P. D. Mitcheson, and S. Lucyszyn, "Ambient RF energy harvesting in urban and semi-urban environments," *IEEE Trans. Microw. Theory Techn.*, vol. 61, no. 7, pp. 2715–2726, Jul. 2013.
[25] A. Collado, S. Daskalakis, K. Niotaki, R. Martinez, F. Bolos, and A. Georgiadis, "Rectifier design challenges for RF wireless power transfer and energy harvesting systems," *Radioengineering*, vol. 26, no. 2, pp. 411–417, Jun. 2017.
[26] A. Boaventura, A. Collado, N. B. Carvalho, and A. Georgiadis, "Optimum behavior: Wireless power transmission system design through behavioral models and efficient synthesis techniques," *IEEE Microw. Mag.*, vol. 14, no. 2, pp. 26–35, Mar./Apr. 2013.
[27] K. Niotaki, S. Kim, S. Jeong, A. Collado, A. Georgiadis, and M. M. Tentzeris, "A compact dual-band rectenna using slot-loaded dual band folded dipole antenna," *IEEE Antennas Wireless Propag. Lett.*, vol. 12, pp. 1634–1637, 2013.
[28] K. Niotaki, A. Georgiadis, A. Collado, and J. S. Vardakas, "Dual-band resistance compression networks for improved rectifier performance," *IEEE Trans. Microw. Theory Techn.*, vol. 62, no. 12, pp. 3512–3521, Dec. 2014.
[29] G. Saini, S. Sarkar, M. Arrawatia, and M. S. Baghini, "Efficient power management circuit for RF energy harvesting with 74.27% efficiency at 623nW available power," in *Proc. IEEE Int. New Circuits Syst. Conf. (NEWCAS)*, Vancouver, BC, Canada, Jun. 2016, pp. 1–4.
[30] X. Chen, L. Huang, J. Xing, Z. Shi, and Z. Xie, "Energy harvesting system and circuits for ambient WiFi energy harvesting," in *Proc. 12th Int. Conf. Comput. Sci. Educ. (ICCSE)*, Houston, TX, USA, Aug. 2017, pp. 769–772.
[31] Z. Zeng, J. J. Estrada-López, M. A. Abouzied, and E. Sánchez-Sinencio, "A reconfigurable rectifier with optimal loading point determination for RF energy harvesting from −22 dBm to −2 dBm," *IEEE Trans. Circuits Syst. II, Exp. Briefs*, vol. 67, no. 1, pp. 87–91, Jan. 2020.
[32] R. V. Prasad, S. Devasenapathy, V. S. Rao, and J. Vazifehdan, "Reincarnation in the ambiance: Devices and networks with energy harvesting," *IEEE Commun. Surveys Tuts.*, vol. 16, no. 1, pp. 195–213, 1st Quart., 2014.
[33] G. V. Merrett and A. S. Weddell, "Supercapacitor leakage in energy-harvesting sensor nodes: Fact or fiction?" in *Proc. 9th Int. Conf. Netw. Sens. (INSS)*, Antwerp, Belgium, Jun. 2012, pp. 1–5.
[34] A. Pegatoquet, T. N. Le, and M. Magno, "A wake-up radio-based MAC protocol for autonomous wireless sensor networks," *IEEE/ACM Trans. Netw.*, vol. 27, no. 1, pp. 56–70, Feb. 2019.
[35] B. Munir and V. Dyo, "On the impact of mobility on battery-less RF energy harvesting system performance," *Sensors*, vol. 18, p. 3597, Oct. 2018.
[36] *Datasheet SHT3x-DIS Humidity and Temperature Sensor*, Sensirion, Stäfa, Switzerland, May 2018.

Joseph Finnegan (Member, IEEE) received the B.Sc. degree in computer science from Maynooth University, Maynooth, Ireland, in 2015, and the M.Sc. degree in computer science from the University of Bristol, Bristol, U.K., in 2016. He is currently pursuing the Ph.D. degree in wireless communications with Maynooth University.

His current research interests include wireless communications and networking, sensor networks, and the Internet of Things.

Kyriaki Niotaki (Member, IEEE) received the B.Sc. degree in informatics and the M.Sc. degree in electronic telecommunications technology from the Aristotle University of Thessaloniki, Thessaloniki, Greece, in 2009 and 2011, respectively, and the Ph.D. degree from the Polytechnic University of Catalonia, Barcelona, Spain, in 2014.

She spent a few years as an RF Design Engineer in industry before returning to academia. She is currently an Assistant Professor with Maynooth University, Maynooth, Ireland. Her research interests lie in the field of 5G microwave circuits and systems and energy harvesting solutions.

Stephen Brown received the B.A.I. degree in electronic engineering and the M.Sc. degree in computer science from the University of Dublin, Dublin, Ireland, in 1982 and 1984, respectively, and the Ph.D. degree from University College Cork, Cork, Ireland, in 2010.

He is currently a Senior Lecturer with Maynooth University, Maynooth, Ireland, where he is a Member of the Irish CONNECT SFI funded research centre. His research interests are in wireless sensor networking and IoT.